ACS APPLIED MATERIALS & INTERFACES

Research Article

www.acsami.org

# Development of Large-Scale Size-Controlled Adult Pancreatic Progenitor Cell Clusters by an Inkjet-Printing Technique

Jia Yang,[†,‡] Fang Zhou,[†,‡] Rubo Xing,[†] Yuan Lin,*[,†] Yanchun Han,[†] Chunbo Teng,*[,§] and Qian Wang[∥]

[†]State Key Laboratory of Polymer Physics and Chemistry, Changchun Institute of Applied Chemistry, Chinese Academy of Sciences, Changchun 130022, P. R. China

[§]College of Life Science, Northeast Forestry University, Harbin 150040, P. R. China

[∥]Department of Chemistry and Biochemistry, University of South Carolina, 631 Sumter Street, Columbia, South Carolina 29208, United States

Supporting Information

**ABSTRACT:** The generation of transplantable $\beta$-cells from pancreatic progenitor cells (PPCs) could serve as an ideal cell-based therapy for diabetes. Because the transplant efficiency depends on the size of islet-like clusters, it becomes one of the key research topics to produce PPCs with controlled cluster sizes in a scalable manner. In this study, we used inkjet printing to pattern biogenic nanoparticles, i.e., mutant tobacco mosaic virus (TMV), with different spot sizes to support the formation of multicellular clusters by PPCs. We successfully achieved TMV particle patterns with variable features and sizes by adjusting the surface wettability and printing speed. The spot sizes of cell-adhesive TMV mutant arrays were in the range of 50−150 $\mu$m diameter. Mouse PPCs were seeded on the TMV-RGD (arginine−glycine−aspartate)-patterned polystyrene (PS) substrate, which consists of areas that either favor (TMV-RGD) or prohibit (bare PS) cell adhesion. The PPCs stably attached, proliferated on top of the TMV-RGD support, thus resulting in the formation of uniform and confluent PPC clusters. Furthermore, the aggregated PPCs also maintained their multipotency and were positive for E-cadherin, indicating that the formation of cell−cell junctions is critical for enhanced cell−cell contact.

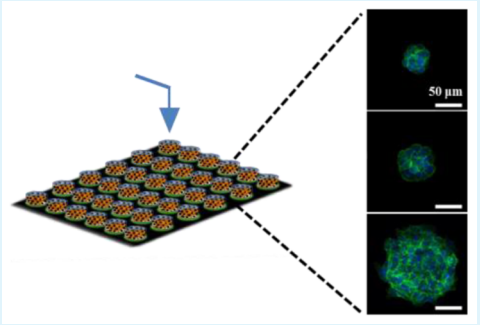


**KEYWORDS:** *tobacco mosaic virus, inkjet printing, surface pattern, pancreatic progenitor cell, cell cluster*

## 1. INTRODUCTION

Diabetes mellitus is a glucose metabolic disorder caused by the autoimmune destruction of $\beta$-cells in the pancreatic islets of Langerhans (type 1 diabetes mellitus) or by a relative $\beta$-cell dysfunction and insulin resistance (type 2 diabetes mellitus). Recently, pancreas or islet transplantation has been considered as a potential treatment for diabetic patients by supporting glucose homeostasis.[1] However, the side effects of toxic immunosuppressive drugs and the limitations of long-term success and especially of the scarcity of donor tissue hampered its widespread use.[2,3]

Pancreatic progenitor cells (PPCs) are promising candidates to generate substituting $\beta$-cells.[4,5] Recent success in the isolation of PPCs has raised expectations that it might be possible to cure diabetes by transplanting PPCs or their mature progenies.[6−9] It is well-known that PPCs function better when they are configured as islet-like clusters,[7,10] possibly because of the improved cell−cell contact. Similarly, pancreatic islet-like cell aggregates have a greater glucose-stimulated insulin release profile than that of single cells.[11] However, it was observed that the viability of cells in the core of larger clusters was affected by nutrient and oxygen deprivation because of the diffusion barriers.[12,13] To overcome this limitation, smaller sizes (50−150 $\mu$m diameter) of islets have been produced, which exhibited increased viability and superior insulin response than larger islets under hypoxia induction.[14] Furthermore, enhanced oxygenation has also been proven to promote the differentiation of $\beta$-cells from PPCs.[15] Therefore, the development of size-controlled PPC clusters will be critical to the fabrication of islet grafts.

In literature, static suspension on nonadhesive surfaces and rotational culture were reported to produce islet-like cell clusters.[8,16] Unfortunately, these methods afforded little control over the cluster size, and irregular cell aggregates often formed in the culture. Alternatively, a hanging-drop technique was reported to create uniform islet clusters with different sizes based upon the cell density per droplet.[17,18] However, this method was limited to a narrow size range for the aggregates and was disadvantageous in the mass preparation because of its laborious procedure. More recently, microwell platform and microcontact printing techniques have been applied to develop

Received: March 27, 2015
Accepted: May 11, 2015
Published: May 11, 2015




DOI: 10.1021/acsami.5b02676
ACS Appl. Mater. Interfaces 2015, 7, 11624−11630

$\beta$-cell clusters of relatively ideal size and shape in a more controllable and efficient manner.[16,19−22]

To develop a culture method that is facile tuning of the cluster size in a high-throughput manner, we introduced inkjet printing as a method for fabricating patterns of materials to direct PPC growth. Inkjet printing can efficiently afford high-throughput, large-area, maskless, and accurate dispensation of synthetic materials, nanoparticles, and functional proteins.[23−25] In particular, because of the noncontact feature of the inkjet-printing technique, contamination can be minimized and the biological activities of biomacromolecules maintained during the printing process.[26,27] Recently, inkjet printing has been adapted to various biomedical applications including cell patterning, tissue engineering, DNA microarrays, protein microarrays, and biosensors.[28−30] Cell patterning was achieved by the direct inkjet printing of cells or by directing the cell behavior through depositing patterns of biomolecules such as cell adhesive proteins.[31,32]

In this paper, we report the feasibility of inkjet printing of anisotropic tobacco mosaic virus (TMV) particles for PPC patterning. TMV is a rodlike nanoparticle that consists of ~2130 identical protein subunits helically arranged around a single-strand RNA, and it is 300 nm in length and 18 nm in diameter.[33] TMV particles represent monodispersed supramolecular assemblies with organized three-dimensional architecture, which can be isolated in high purity with batch-to-batch consistencies in a time-honored fashion at low costs. The surface properties of the virus can be adjusted through chemical or genetic modifications to incorporate polyvalent functional ligands with high density and ordered spatial arrangement.[34,35] Depending on these unique properties, TMV particles have emerged as nanosized building blocks for directing cell growth and differentiation.[36−40] Herein, we report the creation of large-scale surface patterns of TMV particles using a drop-on-demand piezoelectric inkjet printer (Scheme 1). By control of the surface wettability and printing speed, regular TMV arrays with defined shape, dimension, and spacing have been achieved. Finally, we prepared uniformly size-controlled PPC clusters on TMV-RGD (arginine−glycine−aspartate)-patterned surfaces.

**Scheme 1. Schematic Illustration of TMV Patterns That Were Produced by a Single-Nozzle Drop-on-Demand Piezoelectric Inkjet Printer**[a]

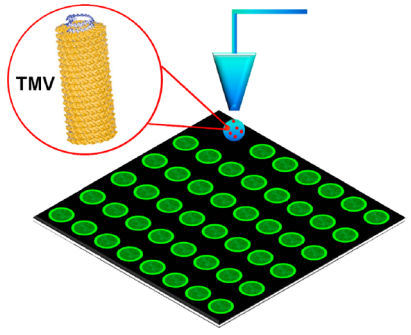


[a]The magnified section shows the structural feature of a rodlike TMV. The model of TMV was generated using PyMol (www.pymol.org) with coordinates obtained from the RCSB Protein Data Bank (www.pdb.org).

## 2. EXPERIMENTAL SECTION

**2.1. Materials.** TMV particles were purified by previously reported methods.[35] A poly(diallyldimethylammonium chloride) (PDDA) aqueous solution ($M_w$ = 200000−350000), sodium poly(styrenesulfonate) (PSS; $M_w$ = 70000), bovine serum albumin (BSA), 4′,6-diamidino-2-phenylindole (DAPI), and fluorescein isothiocyanate (FITC) were purchased from Sigma-Aldrich Co. Polystyrene (PS) was purchased from Aladdin Co. All reagents were used as received without further purification. Ultrapure water (18.2 MΩ) was purified using a UNIQUE-R20 system.

**2.2. Substrate Preparation.** Silicon (Si) wafers were cleaned with a piranha solution (7:3 mixture of 98% $H_2SO_4$ and 30% $H_2O_2$) at 75 °C for 2 h, then washed thoroughly with ultrapure water, and dried with nitrogen gas. The contact angle for the cleaned Si wafer was ~5°. To fabricate different wettabilities of the surfaces, the cleaned Si wafers were modified using PDDA, PSS, BSA, and PS. The cleaned Si wafer was completely immersed in a PDDA solution (2 mg/mL PDDA containing 0.25 M NaCl) for 1 h, then washed thoroughly with ultrapure water, and dried with nitrogen gas. Subsequently, the positively charged surface was immersed in a 2 mg/mL PSS solution for 20 min, then washed thoroughly with ultrapure water, and dried with nitrogen gas. The contact angle for the PDDA/PSS-modified surface was 25 ± 2°. For the BSA-modified surface, the cleaned Si wafer was submerged in a BSA solution (2 mg/mL, pH 4.5) for 2 h, then washed thoroughly with ultrapure water, and dried with nitrogen gas. The contact angle for the BSA-modified surface was 60 ± 2°. For the PS-modified surface, the cleaned Si wafer was spin-coated with 5 mg/mL PS at a speed of 1500 rpm, and the contact angle was 90 ± 1°.

**2.3. Inkjet Printer.** The inkjet printer was equipped with a drop-on-demand piezoelectric inkjet nozzle (Microdrop Technique GmbH, Norderstedt, Germany) with a 70 $\mu$m orifice and a computer-controlled $X-Y$ axis translation stage. The gap between the nozzle and substrate was maintained at 1.0 mm during printing at 25 °C and 40% relative humidity. An individual droplet could be analyzed by a CCD camera equipped with a strobe-LED light. The droplets were jetted at a frequency of 100 Hz with a volume of about 150 pL.

**2.4. Cell Culture.** The mouse adult PPCs were cultured as described in a previous report.[41] Briefly, PPCs were cultured with a 1:1 mixture of a Dulbecco's modified Eagle's medium and F-12 supplemented with 2% fetal bovine serum, 100 U/mL penicillin, 100 $\mu$g/mL streptomycin, 1× B27 (Invitrogen), 1× 2-mercaptoethanol (Gibco), 2 ng/mL EGF (R&D), and 10 $\mu$g/mL insulin (ProSpec) at 37 °C under 5% $CO_2$ in a humidified atmosphere.

**2.5. Cell Seeding and Cluster Formation.** Prior to seeding the cells, the TMV-RGD-patterned PS substrates were treated with UV irradiation for 15 min and then washed for 10 min in sterile phosphate buffered saline (PBS) containing 200 U/mL penicillin and 200 $\mu$g/mL streptomycin. The PS substrates used for the cell culture were untreated PS dishes, which were purchased from Nest Biotechnology Company. Cells were harvested by trypsin−ethylenediaminetetraacetic acid treatment, resuspended in the above media without serum, and seeded on TMV-RGD-printed PS substrates at a density of $2 \times 10^4$ cells/cm$^2$. The cells were allowed to contact with the substrate in an incubator for 3 h. Unattached cells were then removed by rinsing with prewarmed PBS. The cells cultured on the bare PS surfaces as a control were not washed because they were only suspended in the medium. The cells were cultured under static conditions in the incubator for 3 days, changing the media after 2 days. After 3 days of culture, either the cell clusters were imaged or further studies were performed.

**2.6. Immunofluorescence Staining.** The PPCs cultured on the cell patterning substrates were fixed with 4% paraformaldehyde for 30 min at room temperature. After being washed three times with PBS, the fixed cells were treated with PBS containing 1.25 $\mu$g/mL DAPI and 1 $\mu$g/mL FITC−phalloidin to stain the cell nucleus and cytoskeletal structure. The fluorescence images were taken with a confocal laser scanning microscope (LSM 700, Carl Zeiss).

**2.7. Gene Expression of PPC Aggregates.** The total RNA was extracted from cells using a Trizol reagent (Life Technologies, Grand


DOI: 10.1021/acsami.5b02676
ACS Appl. Mater. Interfaces 2015, 7, 11624−11630

**Table 1. Primers Used for RT-PCR**

| gene | forward primer (5′-3′) | reserve primer (5′-3′) |
|---|---|---|
| c-Met | CAGTAATGATCTCAATGGGCAAT | AAATGCCCTCTTCCTATGACTTC |
| Hes1 | TCATGGAGAAGAGGCGAAGG | AGGTCATGGCGTTGATCTGG |
| E-cadherin | CCAACAGGGACAAAGAAACAAAGG | GATGACACGGCATGAGAATAGAGG |
| $\beta$-actin | GGTGGGAATGGGTCAGAAGG | AGGAAGAGGATGCGGCAGTG |

Island, NY) according to the manufacturer's instructions. The quality of the RNA was measured using an Infinite 200 PRO NanoQuant plate reader (Tecan Group Ltd., Männedorf, Switzerland). cDNA synthesis was conducted using a Transcriptor First Strand cDNA Synthesis Kit (Roche USA, Florence, SC). Reverse transcription polymerase chain reactions (RT-PCRs) were performed using specific primers (Table 1) to analyze the expression levels of PPC-marker genes and E-cadherin gene. PCR products were analyzed on 1% agarose gels and visualized using the Gel Imaging System (UVP, LLC, USA).

**2.8. Characterization.** Contact-angle data were collected on a VCA-Optima goniometer (AST Products, Inc., Billerica, MA) for a sessile drop of water with 3 $\mu$L drop size at room temperature. The pattern morphology was acquired from a Zeiss optical microscope and a confocal laser scanning microscope (LSM 700, Carl Zeiss) using differential interference contrast.

## 3. RESULTS AND DISCUSSION

**3.1. Surface Wettability.** When a droplet of a dilute colloidal solution containing dispersed particles evaporates on a solid surface, the outward flow carries the suspended solutes/particles to the contact line, resulting in a ring-shaped deposit pattern; this phenomenon is commonly called the "coffee ring" effect.[42] Deegan et al. demonstrated that the contact-line pinning plays a critical role during the drying process, and the ring size is dependent largely on the surface wettability.[42,43] In order to make growing PPCs with controlled cluster sizes, four surfaces with different hydrophobicities were prepared, including uncoated, PSS-coated, BSA-coated, and PS-coated Si wafers, which showed a water contact angles ($\theta_c$) of ~5°, ~25°, ~60°, and ~90°, respectively. We printed a 4.0 mg/mL solution of TMV in a 0.01 M potassium phosphate buffer on the four different surfaces, respectively. As the water evaporated, TMV particles were carried to the contact line by the outward flow and then deposited onto the surface. Optical microscopy was used to characterize the surface wettability effect on the spot size and overall pattern quality. As shown in Figure 1, under a printing speed of 37.5 mm/s and a line spacing of 500 $\mu$m, ringlike spots were formed and the corresponding diameters of the spots were ~270, ~170, ~135, and ~65 $\mu$m, respectively. Obviously, the spot diameter was dependent on the surface wettability and thus larger on the hydrophilic surface than on the relatively hydrophobic surface. Considering that smaller sizes (50−150 $\mu$m diameter) of islets have been shown to exhibit increased viability and superior insulin response over larger islets under hypoxia induction,[14] both the BSA- and PS-coated Si wafers were chosen for the following study of the substrates.

**3.2. Printing Speed.** The pattern morphology and spatial distribution are also a strong function of the printing speed. The interdrop distance, center-to-center of two adjacent drops along the printing direction, is controlled by the movement speed of the translation stage (i.e., printing speed), which also determines the shapes of the pattern, i.e., spot or stripe.[24] When the distance is large enough, an individual spot can be obtained. On the contrary, narrowing the interdrop distance causes individual droplets to merge with each other. When the distance is smaller than the diameter of the single drop, a continuous stripe formed. Decreasing the distance further causes aggregates and nonuniform stripes to form. As shown in Figure 2a,b, individual regular spot patterns with an average diameter of ~130 $\mu$m could be obtained using higher deposition speeds of 37.5 and 25.0 mm/s on the BSA surfaces. By a continuous decrease of the printing speed, the distance between two adjacent droplets decreased and some irregular spot shapes appeared (Figure 2c,d), which could be attributed to the individual droplets merging with each other. Until the distance became less than the diameter of the single droplet, continuous stripes formed. A well-defined stripe pattern appeared at a printing speed of 6.25 mm/s, as shown in Figure 2e. When the speed was lower than 1.25 mm/s, nonuniform stripes appeared, which was due to the aggregation of the droplets (Figure 2f). The regular spot pattern was obtained on the BSA surface, which was repulsive for cells; however, this surface was limited to a narrow size range.

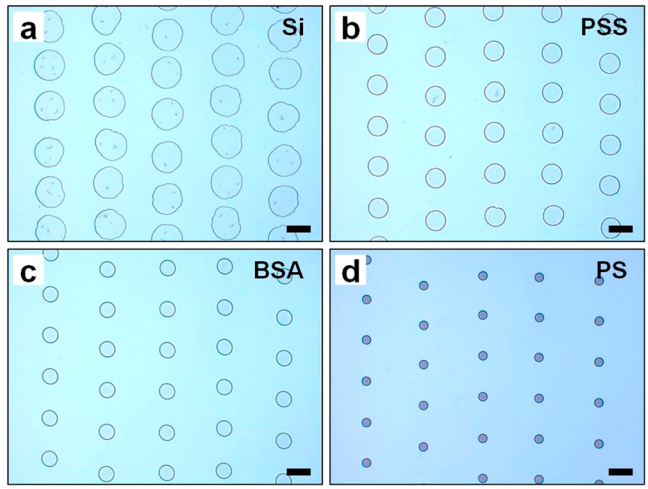


**Figure 1.** Optical images of printed TMV spot patterns on different surfaces: (a) uncoated Si wafer; (b) PSS-coated Si wafer; (c) BSA-coated Si wafer; (d) PS-coated Si wafer. The ink was a 4.0 mg/mL solution of TMV (in a 0.01 M potassium phosphate buffer, pH 7.4). All patterns were generated with a printing speed of 37.5 mm/s, and the line spacing was controlled at 500 $\mu$m. All of the scale bars are 200 $\mu$m.

In order to obtain different-sized spot arrays for cell patterning, we tested the printing speed effect on the relative hydrophobic PS surface, which is also repulsive for cells. Because a droplet could not wet the hydrophobic surface, a stripe pattern would form under the low printing speed; however, the stripe would rupture quickly, and the individual new larger droplets were left on the hydrophobic surface (Figure 3a−c). When the printing speed was high enough, the interdrop distance increased, but the diameter of the individual spots still remained the same (Figure 3d,e). As shown in Figure 3f, after the printing speed reached 12.5 mm/s, the diameter of the individual spots did not change and displayed regular spot


DOI: 10.1021/acsami.5b02676
ACS Appl. Mater. Interfaces 2015, 7, 11624−11630

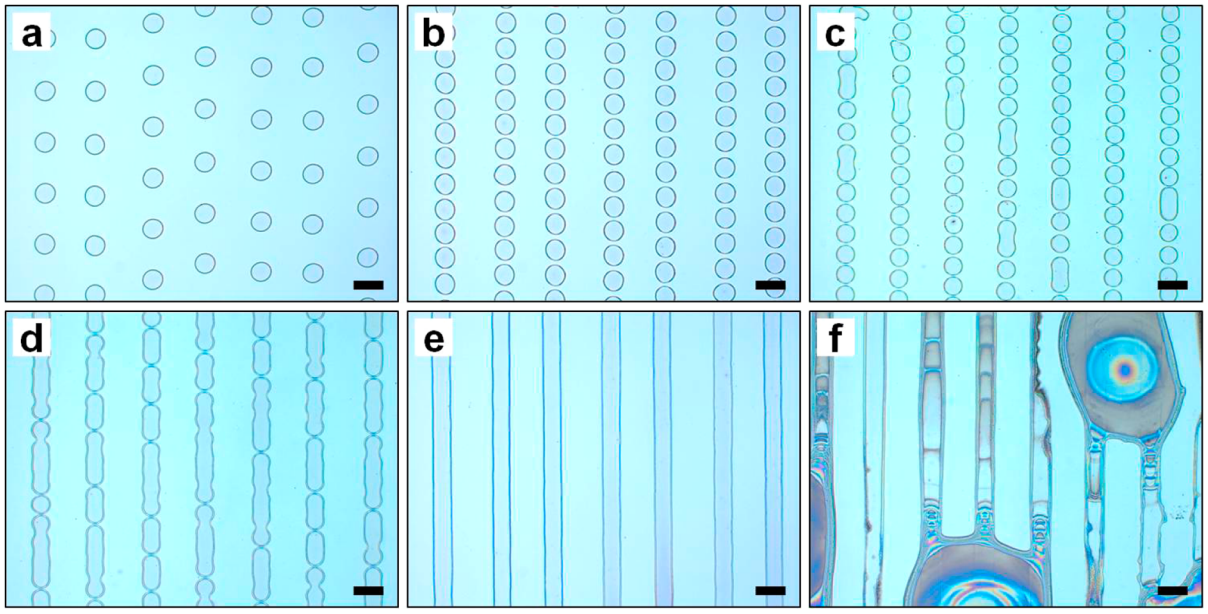


**Figure 2.** Optical images of a printed 4.0 mg/mL solution of TMV (in a 0.01 M potassium phosphate buffer, pH 7.4) on BSA surfaces with varying printing speed: (a) 37.5 mm/s; (b) 25.0 mm/s; (c) 18.75 mm/s; (d) 13.75 mm/s; (e) 6.25 mm/s; (f) 1.25 mm/s. The printing line spacing was controlled at 500 $\mu$m. All of the scale bars are 200 $\mu$m.

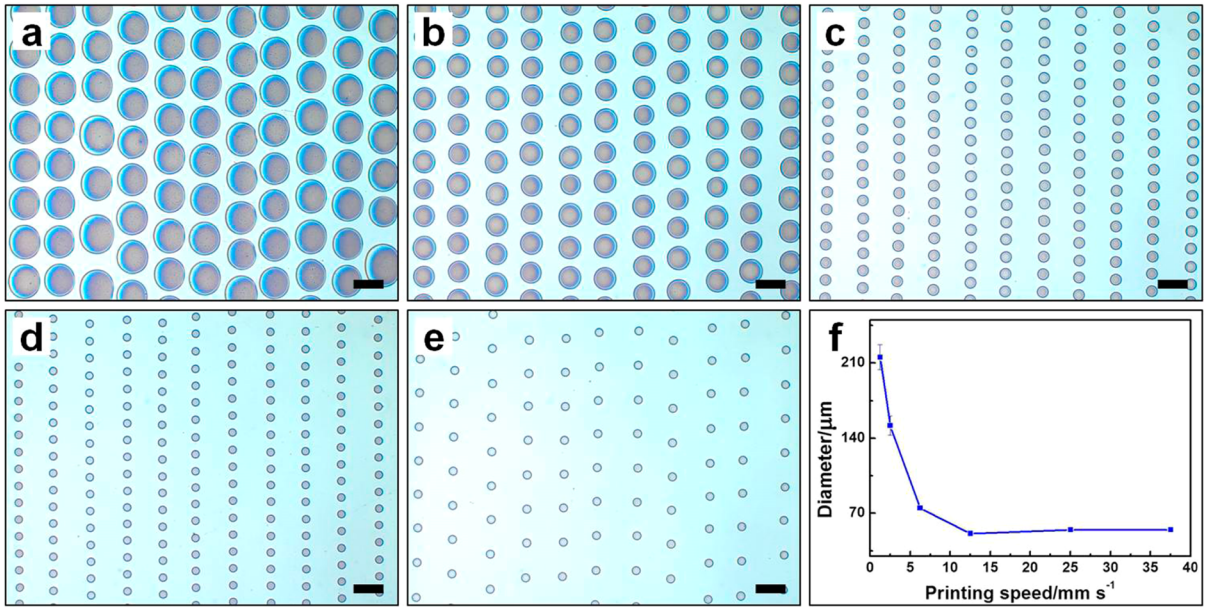


**Figure 3.** Optical images of a printed 1.0 mg/mL solution of TMV (in a 0.01 M potassium phosphate buffer, pH 7.4) on PS surfaces with varying printing speed: (a) 1.25 mm/s; (b) 2.5 mm/s; (c) 6.25 mm/s; (d) 12.5 mm/s; (e) 25.0 mm/s. (f) Change of the spot diameter upon changing printing speed. The printing line spacing was controlled at 250 $\mu$m. All of the scale bars are 200 $\mu$m.

shapes. On the PS surface, the regular spot pattern arrays with diameters in the range of 40−220 $\mu$m were obtained (Figure 3f).

**3.3. Formation of Size-Controlled Cell Clusters.** PPC expansion and differentiation have been proposed as an alternative approach for the generation of insulin-producing $\beta$-cells.[4,41] Given that the cluster size and uniformity are known to influence the islet cell behavior, the capability simple and high-throughput production of size-controlled clusters of PPCs for patients with diabetes could benefit from the growth and differentiation of these cells. Here, utilizing TMV nanoparticle-patterned substrates, we fabricated size-controlled PPC clusters on the surface instead of a suspension culture. To enhance cell adhesion, we used a TMV-RGD mutant in our study that was genetically modified with the RGD (arginine−glycine−aspartate) tripeptide like in our previous report.[44] The active sequence of adhesive proteins RGD has been shown to be critical in islet development in vivo.[45,46] We patterned an untreated PS dish with arrays of TMV-RGD spot patterns in the range of 50−150 $\mu$m diameter. Because untreated PS prevented cell adhesion, the printed TMV-RGD spots served as cell-adhesive microdomains. Prior to cell culture experiments, the stability of the TMV-RGD patterns on PS surfaces was investigated. The TMV-RGD spot pattern printed on the PS


DOI: 10.1021/acsami.5b02676
ACS Appl. Mater. Interfaces 2015, 7, 11624−11630

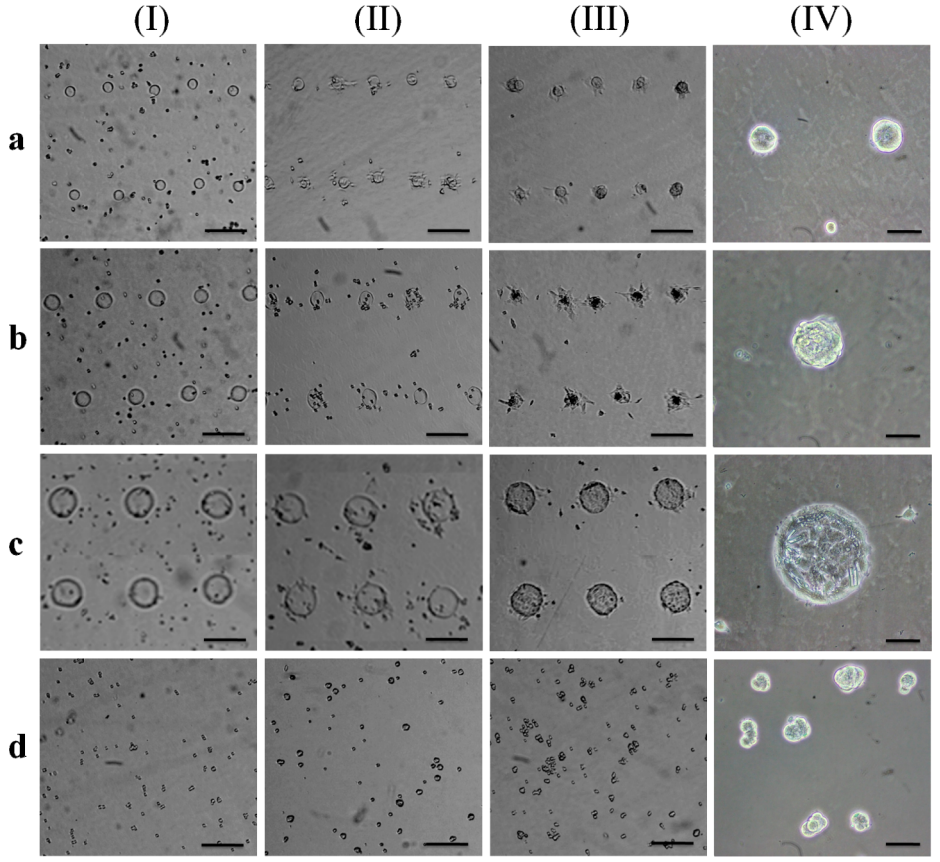


**Figure 4.** Microscopic images illustrating the formation of PPC clusters on TMV-RGD-patterned PS surfaces at 0 h (I), 3 h (II), 24 h (III), and 3 days (IV) after seeding. Inkjet printed 2.0 mg/mL solution of TMV-RGD (in a 0.01 M potassium phosphate buffer, pH 7.4) with varying printing speeds of (a) 10, (b) 5, and (c) 1.25 mm/s and (d) on an untreated PS substrate. The printing line spacing was controlled at 500 $\mu$m. The scale bars of I–III and IV are 200 and 50 $\mu$m, respectively.

surface remained on the surface after incubation in a medium for 7 days (Figure S1 in the SI). PPCs were seeded on the TMV-RGD-patterned PS surfaces at a density of $2.0 \times 10^4$ cells/cm$^2$. The microscopic images of PPCs cultured on the TMV-RGD-spot-patterned PS surfaces, with diameters of approximately 50, 75, and 150 $\mu$m, were recorded at different time points in a serum-free medium. Dispersed single PPCs were seeded, and there were many rounded cells floating randomly in the media [Figure 4a–d(I)]. After 3 h of incubation, PPCs settled and attached preferentially onto the TMV-RGD spot domains. It was clear that the TMV-RGD patterns on the PS substrates provided places for cell adhesion [Figure 4a–c(II)]. PPCs proliferated within the spot patterns and achieved confluent patterns after 24 h, forming circular cell clusters [Figure 4a–c(III)]. As the PPCs further proliferated, we found that the colonies gradually formed cell aggregates at day 3 [Figure 4a–c(IV)]. It was shown that cell patterning was successfully achieved to form circular cell colonies. Figure 5 shows fluorescent microscopy of PPCs cultured on TMV-RGD-patterned substrates with ~50-, 75-, and 150-$\mu$m-diameter spot domains on day 3. We also cultured PPCs on a bare PS substrate as a control. As shown in Figure 4d(I–IV), PPCs spread randomly across the entire surface and aggregated in suspension to form clusters with varying sizes.

**3.4. Gene-Expression Analysis of PPCs Grown on the TMV-RGD-Patterned Substrates.** RT-PCR was conducted to compare the gene expression of PPCs grown on the different size patterns and bare PS substrates for 3 days. The transcriptional levels of PPC markers including c-Met and Hes1 were examined by RT-PCR.[41,47] c-Met is considered to be a general PPC marker and plays an important role in the progenitor cell function in both the developing and adult pancreas.[47] Hes1 also is molecular marker of PPCs and operates as a general negative regulator of endodermal endocrine differentiation.[48,49] PPCs cultured on TMV-RGD-patterned substrates with different sizes as well as on bare PS substrates exhibited similar transcriptional levels of the marker genes (Figure 6). This result demonstrated that PPC clusters on the TMV-RGD-patterned surfaces maintained the gene-expression signatures of PPCs and they potentially could be further induced to differentiate pancreatic endocrine cells under the endocrine differentiation condition. In addition, compared to the cells cultured on bare PS substrates, PPC clusters forming on TMV-RGD-patterned substrates had significantly high expression of the E-cadherin gene, especially on the larger size 150 $\mu$m spot surfaces with a printing speed of 1.25 mm/s. E-cadherin is a cell surface adhesion protein that facilitates cell–cell contact.[50] This indicated that the clusters forming on the TMV-RGD pattern could afford sufficient cell–cell contact and promote the formation of cell–cell junctions. The improved cellular contact could be important for preserving the cell viability, function, and proper signaling.

## 4. CONCLUSIONS

In conclusion, we describe a method for the fabrication of uniformly size-controlled PPC clusters on viral nanoparticle-


DOI: 10.1021/acsami.5b02676
ACS Appl. Mater. Interfaces 2015, 7, 11624–11630

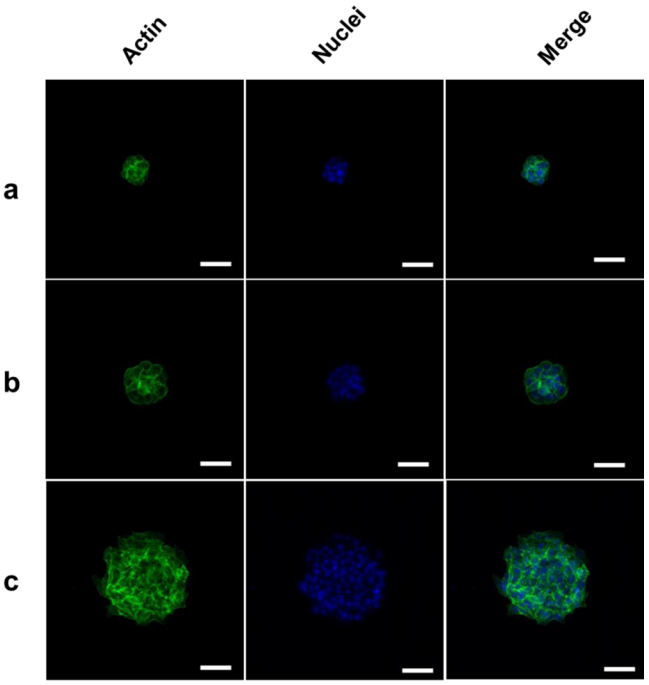


**Figure 5.** Aggregated PPC clusters on TMV-RGD-patterned PS substrates. The cell seeding density was $2.0 \times 10^4$ cells/cm$^2$. Confocal images were taken 3 days after seeding. Inkjet printed 2.0 mg/mL solution of TMV-RGD (in a 0.01 M potassium phosphate buffer, pH 7.4) with varying printing speeds of (a) 10, (b) 5, and (c) 1.25 mm/s. Color code: green, F-actin−phalloidin stain; blue, DAPI nuclear stain. The scale bars are 50 $\mu$m.

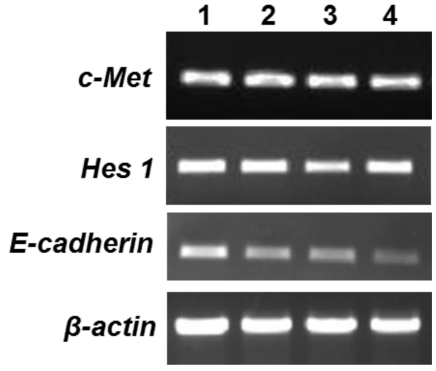


**Figure 6.** PPCs cultured on TMV-RGD-patterned substrates and untreated PS substrates for 3 days. RNA was extracted, and the expressions of PPC markers and E-cadherin were analyzed by RT-PCR. Inkjet printed 2.0 mg/mL solution of TMV-RGD (in a 0.01 M potassium phosphate buffer, pH 7.4) with varying printing speeds of (1) 1.25, (2) 5, and (3) 10 mm/s and (4) on an untreated PS substrate. The printing line spacing was controlled at 500 $\mu$m.

patterned surfaces using inkjet-printing technology. The cluster size correlated with the spot dimensions, which were controlled by varying the printing speed. We found that TMV-RGD-patterned substrates not only supported PPC growth and multipotency but also promoted intracellular contact. We envision that this platform will afford a facile way to produce uniformly clustered pancreatic progenitors and has great potential in antidiabetic cell-based therapies.

## ■ ASSOCIATED CONTENT

### Ⓢ Supporting Information

Stability of TMV-RGD patterns on PS surfaces. The Supporting Information is available free of charge on the ACS Publications website at DOI: 10.1021/acsami.5b02676.

## ■ AUTHOR INFORMATION

### Corresponding Authors

* E-mail: linyuan@ciac.ac.cn.
* E-mail: chunboteng@nefu.edu.cn.

### Author Contributions

‡These authors contributed equally.

### Notes

The authors declare no competing financial interest.

## ■ ACKNOWLEDGMENTS

This work is supported by the National Natural Science Foundation of China (Grants 21374119, 21429401, and 20990233).

## ■ REFERENCES

(1) Shapiro, A. M. J.; Lakey, J. R. T.; Ryan, E. A.; Korbutt, G. S.; Toth, E.; Warnock, G. L.; Kneteman, N. M.; Rajotte, R. V. Islet Transplantation in Seven Patients with Type 1 Diabetes Mellitus Using a Glucocorticoid-free Immunosuppressive Regimen. *N. Engl. J. Med.* **2000**, *343*, 230−238.

(2) Ichii, H.; Ricordi, C. Current Status of Islet Cell Transplantation. *J. Hepatopancreatobiliary Surg.* **2009**, *16*, 101−112.

(3) Rother, K. I.; Harlan, D. M. Challenges Facing Islet Transplantation for the Treatment of Type 1 Diabetes Mellitus. *J. Clin. Invest.* **2004**, *114*, 877−883.

(4) Noguchi, H. Pancreatic Stem/Progenitor Cells for the Treatment of Diabetes. *Rev. Diabet Stud.* **2010**, *7*, 105−111.

(5) Lysy, P. A.; Weir, G. C.; Bonner-Weir, S. Concise Review: Pancreas Regeneration: Recent Advances and Perspectives. *Stem Cells Transl. Med.* **2012**, *1*, 150−159.

(6) Lysy, P. A.; Weir, G. C.; Bonner-Weir, S. Making beta Cells From Adult Cells within the Pancreas. *Curr. Diabetes Rep.* **2013**, *13*, 695−703.

(7) Seaberg, R. M.; Smukler, S. R.; Kieffer, T. J.; Enikolopov, G.; Asghar, Z.; Wheeler, M. B.; Korbutt, G.; van der Kooy, D. Clonal Identification of Multipotent Precursors from Adult Mouse Pancreas that Generate Neural and Pancreatic Lineages. *Nat. Biotechnol.* **2004**, *22*, 1115−1124.

(8) Kruse, C.; Kajahn, J.; Petschnik, A. E.; Maaß, A.; Klink, E.; Rapoport, D. H.; Wedel, T. Adult Pancreatic Stem/Progenitor Cells Spontaneously Differentiate in Vitro into Multiple Cell Lineages and Form Teratoma-like Structures. *Ann. Anat.* **2006**, *188*, 503−517.

(9) Xu, X.; D'Hoker, J.; Stange, G.; Bonne, S.; De Leu, N.; Xiao, X.; De Casteele, M. V.; Mellitzer, G.; Ling, Z.; Pipeleers, D.; Bouwens, L.; Scharfmann, R.; Gradwohl, G.; Heimberg, H. Beta Cells can be Generated from Endogenous Progenitors in Injured Adult Mouse Pancreas. *Cell* **2008**, *132*, 197−207.

(10) Ramiya, V. K.; Maraist, M.; Arfors, K. E.; Schatz, D. A.; Peck, A. B.; Cornelius, J. G. Reversal of Insulin-Dependent Diabetes using Islets Generated in Vitro From Pancreatic Stem Cells. *Nat. Med.* **2000**, *6*, 278−282.

(11) Matta, S. G.; Wobken, J. D.; Williams, F. G.; Bauer, G. E. Pancreatic Islet Cell Reaggregation Systems: Efficiency of Cell Reassociation and Endocrine Cell Topography of Rat Islet-like Aggregates. *Pancreas* **1994**, *9*, 439−449.

(12) Ramachandran, K.; Williams, S. J.; Huang, H.-H.; Novikova, L.; Stehno-Bittel, L. Engineering Islets for Improved Performance by Optimized Reaggregation in a Micromold. *Tissue Eng., Part A* **2013**, *19*, 604−612.



DOI: 10.1021/acsami.5b02676
*ACS Appl. Mater. Interfaces* 2015, 7, 11624−11630

(13) O'Sullivan, E. S.; Vegas, A.; Anderson, D. G.; Weir, G. C. Islets Transplanted in Immunoisolation Devices: A Review of the Progress and the Challenges that Remain. *Endocr. Rev.* **2011**, *32*, 827−844.
(14) Lehmann, R.; Zuellig, R. A.; Kugelmeier, P.; Baenninger, P. B.; Moritz, W.; Perren, A.; Clavien, P. A.; Weber, M.; Spinas, G. A. Superiority of Small Islets in Human Islet Transplantation. *Diabetes* **2007**, *56*, 594−603.
(15) Fraker, C. A.; Álvarez, S.; Papadopoulos, P.; Giraldo, J.; Gu, W.; Ricordi, C.; Inverardi, L.; Domínguez-Bendala, J. Enhanced Oxygenation Promotes $\beta$-Cell Differentiation In Vitro. *Stem Cells* **2007**, *25*, 3155−3164.
(16) Gallego-Perez, D.; Higuita-Castro, N.; Reen, R. K.; Palacio-Ochoa, M.; Sharma, S.; Lee, L. J.; Lannutti, J. J.; Hansford, D. J.; Gooch, K. J. Micro/nanoscale Technologies for the Development of Hormone-expressing Islet-like Cell Clusters. *Biomed. Microdevices* **2012**, *14*, 779−789.
(17) Cavallari, G.; Zuellig, R. A.; Lehmann, R.; Weber, M.; Moritz, W. Rat Pancreatic Islet Size Standardization by the "Hanging Drop" Technique. *Transplant. Proc.* **2007**, *39*, 2018−2020.
(18) Kim, H. J.; Alam, Z.; Hwang, J. W.; Hwang, Y. H.; Kim, M. J.; Yoon, S.; Byun, Y.; Lee, D. Y. Optimal Formation of Genetically Modified and Functional Pancreatic Islet Spheroids by Using Hanging-Drop Strategy. *Transplant. Proc.* **2013**, *45*, 605−610.
(19) Mendelsohn, A. D.; Bernards, D. A.; Lowe, R. D.; Desai, T. A. Patterning of Mono- and Multilayered Pancreatic beta-Cell Clusters. *Langmuir* **2010**, *26*, 9943−9949.
(20) Van Hoof, D.; Mendelsohn, A. D.; Seerke, R.; Desai, T. A.; German, M. S. Differentiation of Human Embryonic Stem Cells into Pancreatic Endoderm in Patterned Size-Controlled Clusters. *Stem Cell Res.* **2011**, *6*, 276−285.
(21) Mendelsohn, A. D.; Nyitray, C.; Sena, M.; Desai, T. A. Size-Controlled Insulin-secreting Cell Clusters. *Acta Biomater.* **2012**, *8*, 4278−4284.
(22) Bernard, A. B.; Lin, C.-C.; Anseth, K. S. A Microwell Cell Culture Platform for the Aggregation of Pancreatic beta-Cells. *Tissue Eng., Part C* **2012**, *18*, 583−592.
(23) Minemawari, H.; Yamada, T.; Matsui, H.; Tsutsumi, J.; Haas, S.; Chiba, R.; Kumai, R.; Hasegawa, T. Inkjet Printing of Single-crystal Films. *Nature* **2011**, *475*, 364−367.
(24) Park, J.; Moon, J. Control of Colloidal Particle Deposit Patterns within Picoliter Droplets Ejected by Ink-jet Printing. *Langmuir* **2006**, *22*, 3506−3513.
(25) Derby, B. Bioprinting: Inkjet Printing Proteins and Hybrid Cell-containing Materials and Structures. *J. Mater. Chem.* **2008**, *18*, 5717−5721.
(26) Yang, S.; Wang, C. F.; Chen, S. A Release-induced Response for the Rapid Recognition of Latent Fingerprints and Formation of Inkjet-printed Patterns. *Angew. Chem., Int. Ed.* **2011**, *50*, 3706−3709.
(27) Boland, T.; Xu, T.; Damon, B.; Cui, X. Application of Inkjet Printing to Tissue Engineering. *Biotechnol. J.* **2006**, *1*, 910−917.
(28) Saunders, R. E.; Derby, B. Inkjet Printing Biomaterials for Tissue Engineering: Bioprinting. *Int. Mater. Rev.* **2014**, *59*, 430−448.
(29) Sakurai, K.; Teramura, Y.; Iwata, H. Cells Immobilized on Patterns Printed in DNA by an Inkjet Printer. *Biomaterials* **2011**, *32*, 3596−3602.
(30) Kim, J. D.; Choi, J. S.; Kim, B. S.; Choi, Y. C.; Cho, Y. W. Piezoelectric Inkjet Printing of Polymers: Stem Cell Patterning on Polymer Substrates. *Polymer* **2010**, *51*, 2147−2154.
(31) Roth, E. A.; Xu, T.; Das, M.; Gregory, C.; Hickman, J. J.; Boland, T. Inkjet Printing for High-throughput Cell Patterning. *Biomaterials* **2004**, *25*, 3707−3715.
(32) Zarowna-Dabrowska, A.; McKenna, E. O.; Schutte, M. E.; Glidle, A.; Chen, L.; Cuestas-Ayllon, C.; Marshall, D.; Pitt, A.; Dawson, M. D.; Gu, E.; Cooper, J. M.; Yin, H. Generation of Primary Hepatocyte Microarrays by Piezoelectric Printing. *Colloids Surf., B* **2012**, *89*, 126−132.
(33) Shenton, W.; Douglas, T.; Young, M.; Stubbs, G.; Mann, S. Inorganic−organic Nanotube Composites from Template Mineralization of Tobacco Mosaic Virus. *Adv. Mater.* **1999**, *11*, 253−256.
(34) Kaur, G.; Wang, C.; Sun, J.; Wang, Q. The Synergistic Effects of Multivalent Ligand Display and Nanotopography on Osteogenic Differentiation of Rat Bone Marrow Stem Cells. *Biomaterials* **2010**, *31*, 5813−5824.
(35) Wu, L.; Zang, J.; Lee, L. A.; Niu, Z.; Horvatha, G. C.; Braxtona, V.; Wibowo, A. C.; Bruckman, M. A.; Ghoshroy, S.; zur Loye, H.-C.; Li, X.; Wang, Q. Electrospinning Fabrication, Structural and Mechanical Characterization of Rod-like Virus-based Composite Nanofibers. *J. Mater. Chem.* **2011**, *21*, 8550−8557.
(36) Lin, Y.; Balizan, E.; Lee, L. A.; Niu, Z.; Wang, Q. Self-Assembly of Rodlike Bio-nanoparticles in Capillary Tubes. *Angew. Chem., Int. Ed.* **2010**, *49*, 868−872.
(37) Lin, Y.; Su, Z.; Xiao, G.; Balizan, E.; Kaur, G.; Niu, Z.; Wang, Q. Self-Assembly of Virus Particles on Flat Surfaces via Controlled Evaporation. *Langmuir* **2011**, *27*, 1398−1402.
(38) Sitasuwan, P.; Lee, L. A.; Bo, P.; Davis, E. N.; Lin, Y.; Wang, Q. A Plant Virus Substrate Induces Early Upregulation of BMP2 for Rapid Bone Formation. *Integr. Biol.* **2012**, *4*, 651−660.
(39) Zan, X.; Feng, S.; Balizan, E.; Lin, Y.; Wang, Q. Facile Method for Large Scale Alignment of One Dimensional Nanoparticles and Control over Myoblast Orientation and Differentiation. *ACS Nano* **2013**, *7*, 8385−8396.
(40) Zhao, X.; Lin, Y.; Wang, Q. Virus-based Scaffolds for Tissue Engineering Applications. *Wiley Interdiscip. Rev.: Nanomed. Nanobiotechnol.* **2014**, DOI: 10.1002/wnan.1327.
(41) Zhang, Z.; Zhang, L.; Ding, L.; Wang, F.; Sun, Y.; An, Y.; Zhao, Y.; Li, Y.; Teng, C. MicroRNA-19b Downregulates Insulin 1 through Targeting Transcription Factor NeuroD1. *FEBS Lett.* **2011**, *585*, 2592−2598.
(42) Deegan, R. D.; Bakajin, O.; Dupont, T. F.; Huber, G.; Nagel, S. R.; Witten, T. A. Capillary Flow as the Cause of Ring Stains from Dried Liquid Drops. *Nature* **1997**, *389*, 827−829.
(43) Deegan, R. D.; Bakajin, O.; Dupont, T. F.; Huber, G.; Nagel, S. R.; Witten, T. A. Contact Line Deposits in an Evaporating Drop. *Phys. Rev. E* **2000**, *62*, 756−765.
(44) Lee, L. A.; Nguyen, Q. L.; Wu, L.; Horyath, G.; Nelson, R. S.; Wang, Q. Mutant Plant Viruses with Cell Binding Motifs Provide Differential Adhesion Strengths and Morphologies. *Biomacromolecules* **2012**, *13*, 422−431.
(45) Cirulli, V.; Beattie, G. M.; Klier, G.; Ellisman, M.; Ricordi, C.; Quaranta, V.; Frasier, F.; Ishii, J. K.; Hayek, A.; Salomon, D. R. Expression and Function of Alpha(v)beta(3) and Alpha(v)beta(5) Integrins in the Developing Pancreas: Roles in the Adhesion and Migration of Putative Endocrine Progenitor Cells. *J. Cell Biol.* **2000**, *150*, 1445−1459.
(46) Dubiel, E. A.; Kuehn, C.; Wang, R.; Vermette, P. In Vitro Morphogenesis of PANC-1 Cells into Islet-like Aggregates using RGD-covered Dextran Derivative Surfaces. *Colloids Surf., B* **2012**, *89*, 117−125.
(47) Suzuki, A.; Nakauchi, H.; Taniguchi, H. Prospective Isolation of Multipotent Pancreatic Progenitors Using Flow-cytometric Cell Sorting. *Diabetes* **2004**, *53*, 2143−2152.
(48) Norgaard, G. A.; Jensen, J. N.; Jensen, J. FGF10 Signaling Maintains the Pancreatic Cell State Revealing a Novel Role of Notch in Organ Development. *Dev. Biol.* **2003**, *264*, 323−338.
(49) Jensen, J.; Pedersen, E. E.; Galante, P.; Hald, J.; Heller, R. S.; Ishibashi, M.; Kageyama, R.; Guillemot, F.; Serup, P.; Madsen, O. D. Control of Endodermal Endocrine Development by Hes-1. *Nat. Genet.* **2000**, *24*, 36−44.
(50) Rogers, G. J.; Hodgkin, M. N.; Squires, P. E. E-cadherin and Cell Adhesion: A Role in Architecture and Function in the Pancreatic Islet. *Cell. Physiol. Biochem.* **2007**, *20*, 987−994.


DOI: 10.1021/acsami.5b02676
*ACS Appl. Mater. Interfaces* 2015, 7, 11624−11630